Journal of Fluids and Structures (2000) **14,** 1053–1069
doi:10.1006/jfls.2000.0312, available online at http://www.idealibrary.com on IDEAL®

COMPUTATION OF COBBLESTONE EFFECT WITH UNSTEADY VISCOUS FLOW UNDER A STERN SEAL BAG OF A SES

N. HIRATA

Ship Performance Division, Ship Research Institute, 6-38-1, Shinkawa Tokyo 181-0004, Japan

AND

O. M. FALTINSEN

Norwegian University of Science and Technology, Trondheim, Norway

(Received 26 January 1999, and in final form 25 April 2000)

The concept of a surface effect ship (SES) is to lift the hull partly by the air cushion enclosed within two side hulls, a bow skirt and a stern seal. Consequently, it results in lower draft, resistance and motions than equivalent length catamarans in most sea states. In very low sea states, however, there is a significant design problem, which is high vertical accelerations, referred to as the cobblestone effect. The oscillations are based on resonance phenomena and are caused by the change of the cushion volume due to the incident waves. The resonance oscillations have an important damping mechanism which is derived from the air leakage flow under the stern seal bag of a SES. Hence, the accurate prediction of the leakage flow is required for the estimation of the cobblestone effect. In order to solve the unsteady flow field under the stern seal bag, a viscous flow code for numerically simulating two-dimensional incompressible flows has been developed. The governing equations to be solved are the time-dependent Navier–Stokes equations, using the artificial compressibility approach. The spatial discretization is based on a cell-centred finite volume formulation. The inviscid fluxes are evaluated by Roe's scheme with the third-order-accurate MUSCL approach. Time integration is conducted by the second-order accurate backward Euler formula and the linear equation system is solved by an approximate Newton relaxation scheme with the symmetric Gauss–Seidel iteration approach. For the resulting time integration to be conservative on a moving grid system, a geometric conservation law is introduced. A numerical procedure is presented and contributions of the viscous effects to the cobblestone effect problem are discussed.

© 2000 Academic Press

1. INTRODUCTION

A SURFACE EFFECT SHIP (SES) is an air-cushion-supported high-speed craft where the air-cushion is enclosed with two side hulls, a bow skirt and a stern seal. Due to the support system, one obtains lower draft, resistance and motions than equivalent length catamarans in most sea states. In very low sea-states, however, resonant heave and pitch motions induced by the compressibility of air in the pressurized cushion may produce high vertical accelerations which are referred to as the cobblestone effect. The oscillations are caused by the change of the cushion volume due to the incident waves. The two lowest cushion resonance frequencies for a 30–35 m long SES are approximately 2 and 5–6 Hz, whose pressure variations in the cushion are uniform and the first spatial resonance of a standing wave, respectively.

0889–9746/00/101053 + 17 $35.00/0 © 2000 Academic Press

Ulstein (1995) investigated the nonlinear effects of the bag on the cobblestone effect problem by conducting time-domain simulations coupled with bag motion, cushion pressure and SES motions in the vertical plane. He found that the flexible stern bag reduces the frequency of the first spatial pressure resonance of the air-cushion from 6 to 5 Hz for a 30–35 m long SES, relative to the air-cushion supported with a rigid stern seal. Consequently, prediction of the unsteady pressure distribution on the bag, which is required for the calculation of the bag deformation, is very important in the estimation of the vertical oscillations. Since, however, he assumed that the flow around the bag is inviscid, boundary layers developed over the bag were neglected and the separation point on the bag had to be chosen.

In the present work, the unsteady pressure distribution on the rigid stern seal bag is numerically simulated with consideration of viscous effects. A viscous flow code for a moving grid system has been developed to obtain the solution of the time-dependent Navier–Stokes equations with the artificial compressibility approach. Results are compared with data obtained by Ulstein's method, and the contributions of the viscous effects to the cobblestone effect are discussed.

2. FORMULATION

2.1. Longitudinal Motion Equations for SES

A Cartesian coordinate system, whose origin is at the centre of gravity of the SES, is moving with the forward speed U as defined in Figure 1. The equations of coupled heave η_3 and pitch η_5 motions can be written as

$$(M + A^h_{33})\frac{d^2\eta_3}{dT^2} + B^h_{33}\frac{d\eta_3}{dT} + C^h_{33}\eta_3 + A^h_{35}\frac{d^2\eta_5}{dT^2} + B^h_{35}\frac{d\eta_5}{dT} + C^h_{35}\eta_5 = F^h_3(T) + F^a_3(T) \tag{1}$$

and

$$(I_5 + A^h_{55})\frac{d^2\eta_5}{dT^2} + B^h_{55}\frac{d\eta_5}{dT} + C^h_{55}\eta_5 + A^h_{53}\frac{d^2\eta_3}{dT^2} + B^h_{53}\frac{d\eta_3}{dT} + C^h_{53}\eta_3 = F^h_5(T) + F^a_5(T), \tag{2}$$

where M and I_5 are the mass and moment of inertia of the SES and T is time; A^h, B^h, C^h are the hydrodynamic derivatives of the two side hulls and F^h are linear hydrodynamic

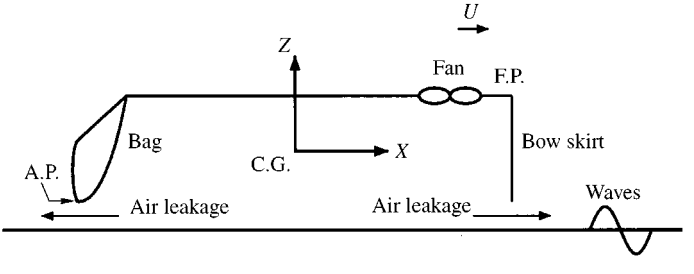

Figure 1. Global coordinate system and cushion model.

excitation forces on the side hulls, which are computed on the basis of the strip theory, as shown by Ulstein (1995).

F^a are nonlinear aerodynamic forces on the SES, defined as

$$F_3^a = B_C \left\{ \int_{\text{cushion}} \hat{P}_C \, \mathrm{d}X + \int_{\text{bag}} \hat{P}_B \, \mathrm{d}X \right\}, \tag{3}$$

$$F_5^a = -B_C \left\{ \int_{\text{cushion}} \hat{P}_C X \, \mathrm{d}X + \int_{\text{bag}} \hat{P}_B X \, \mathrm{d}X \right\}, \tag{4}$$

where B_C is the breadth of the cushion. $\hat{P}_C$ and $\hat{P}_B$ are small perturbations of the cushion pressure and the pressure acting on the bag due to the leakage flow, respectively. The methods to predict these aerodynamic forces are described in Sections 2.2 and 2.3.

In the present scheme, the fourth-order accurate Runge–Kutta method with Gill constants is used as the time integration.

2.2. Air-Flow in a Cushion

2.2.1. *Governing equation*

In order to obtain the aerodynamic forces due to the cushion pressure in equations (3) and (4), the flow in the cushion is solved with use of a time-dependent compressible potential solver. The cushion pressure is assumed to be constant in the lateral and vertical directions. Thus, the linearized one-dimensional governing equation for the air-cushion velocity potential Φ is given by

$$\frac{\partial^2 \Phi}{\partial T^2} - c^2 \frac{\partial^2 \Phi}{\partial X^2} = c^2 \frac{\partial}{\partial Z}\left(\frac{\partial \Phi}{\partial Z}\right), \tag{5}$$

where c is a sound speed and $\partial\Phi/\partial Z$ is given.

The Cushion pressure P_C and air density ρ_C are decomposed as follows:

$$P_C = P_{C0} + \hat{P}_C, \qquad \rho_C = \rho_{C0} + \hat{\rho}_C. \tag{6}$$

In equation (6), the suffix 0 and $\hat{}$ refer to the equilibrium value and perturbation, respectively. Here $\hat{P}_C$ is written as

$$\hat{P}_C = -\rho_{C0} \frac{\partial \Phi}{\partial T}. \tag{7}$$

2.2.2. *Discretization*

A finite-volume approach with a cell-centred layout is adopted for spatial discretization. The velocity potential Φ_i is placed at the centre of each grid cell. The second derivative with respect to X is evaluated with the second-order accurate central differencing scheme. The discretized governing equation is expressed as

$$\frac{\partial^2 \Phi_i}{\partial T^2} = c^2 \left\{ \frac{\Phi_{i+1} - 2\Phi_i + \Phi_{i-1}}{(\Delta X)^2} + \frac{(\partial \Phi_i/\partial Z)_{\text{top}} - (\partial \Phi_i/\partial Z)_{\text{bot}}}{H_C} \right\}, \tag{8}$$

where Φ_i is the average of Φ over Z and H_C is the cushion height.

The time integration scheme used is also the fourth-order accurate Runge–Kutta method with Gill constants, the same for the SES motion equations.

2.2.3. *Boundary conditions*

With consideration of the fan effect, the vertical velocity at the rigid part of the wet deck(top) is defined as

$$\left(\frac{\partial \Phi}{\partial Z}\right)_{\text{top}} = \frac{\mathrm{d}\eta_3}{\mathrm{dT}} - X\frac{\mathrm{d}\eta_5}{\mathrm{d}T} - \frac{(\partial Q_i/\partial P)_0 \hat{P}_C}{A_f}\,\delta(X - X_f), \tag{9}$$

where $(\partial Q_i/\partial P)_0$ is a two-dimensional cushion fan slope at the equilibrium state and X_f, A_f are X coordinates of fan and fan area, respectively. The volume flux of air into the cushion through the fan, Q_i, is decomposed as

$$Q_i = Q_{i0} + \left(\frac{\partial Q_i}{\partial P}\right)_0 \hat{P}_C. \tag{10}$$

The vertical velocity at the free surface (bottom) is given by

$$\left(\frac{\partial \Phi}{\partial Z}\right)_{\text{bot}} = \sum_{n=1}^{N_w} \omega_n \zeta_{an} \cos\left\{k_n\left(\frac{L}{2} - X\right) - \omega_{en}T + \varepsilon_n\right\}, \tag{11}$$

where N_w is the number of regular wave components used. The incident wave amplitude ζ_a is computed from a modified Pierson–Moskowitz wave spectrum; k, ω_e and ε are the wave number, wave encounter frequency and random-phase angle, respectively.

At both bow and stern ends, the longitudinal velocities are expressed as

$$\frac{\partial \Phi}{\partial X} = \frac{Q_o - Q_{o0}}{H_C}, \tag{12}$$

where the volume flux of air leakage, Q_o, is

$$Q_o = V_A k H_L. \tag{13}$$

In the equation above, V_A is the leakage velocity, k is the jet contraction coefficient and H_L is the leakage height. V_A can be computed from the steady Bernoulli's equation for the incompressible flow, since the leakage velocity is smaller than the sound speed, and the length of the seal is much shorter than that of a standing pressure wave in the cushion, so that

$$V_A = \sqrt{\frac{2((P_C)_{\text{end}} - P_a)}{\rho_a(1 - (kH_L/H_C)^2)}}. \tag{14}$$

Here $(P_C)_{\text{end}}$ and P_a are the cushion pressure at bow or stern end and atmospheric pressure, respectively. Equation (14) is derived under the assumption that the flow shifts to a jet flow at the lowest point of the bag.

2.3. Air-Flow Under a Stern Seal Bag

In order to obtain the aerodynamic forces due to the pressure acting on the bag in equations (3) and (4), the pressure distribution on the bag is required. However, predicting the pressure distribution is very difficult, since the leakage flow phenomena around the lowest point of the bag are very complicated. Upstream of the lowest point, the characteristics of the flow are almost the same as those of nozzle flow. When the air passes under the lowest point, the state of the flow changes to diffuser flow. Thus, the flow becomes unstable and the air soon

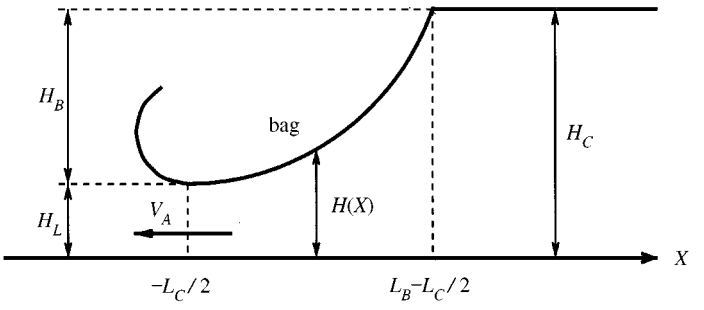

Figure 2. Flow around a stern seal bag.

separates. After the separation, the flow shifts to jet flow. This is considered to characterize the flow phenomena. In the present work, a two-dimensional time-dependent incompressible Navier–Stokes solver is adopted for the investigation of the flow around the bag. Details are described in Section 3.

For comparison, with the steady Bernoulli and continuity equations, the pressure distribution on the bag is computed as follows:

$$P_B(X) = P_a + \frac{1}{2}\rho_a V_A^2 \left\{1 - \left(\frac{k_{AE} H_L}{H(X)}\right)^2\right\}, \tag{15}$$

where $H(X)$ is the ground height as defined in Figure 2.

3. NAVIER–STOKES SOLVER

3.1. Governing Equations

The governing equations are the artificial compressibility form of the two-dimensional time-dependent Navier–Stokes equations in conservative form. They can be given as

$$\frac{\partial \boldsymbol{q}}{\partial t} + \frac{\partial(\boldsymbol{e} + \boldsymbol{e}_v)}{\partial x} + \frac{\partial(\boldsymbol{f} + \boldsymbol{f}_v)}{\partial y} = \boldsymbol{0}, \tag{16}$$

where x and y are the Cartesian coordinates. The dependent variables $\boldsymbol{q}$, the inviscid fluxes $\boldsymbol{e}, \boldsymbol{f}$ and the viscous fluxes $\boldsymbol{e}_v, \boldsymbol{f}_v$ are written as

$$\boldsymbol{q} = \begin{bmatrix} p \\ u \\ v \end{bmatrix}, \quad [\boldsymbol{e}, \boldsymbol{f}] = \begin{bmatrix} \beta u & \beta v \\ u(u - u_g) + p & u(v - v_g) \\ v(u - u_g) & v(v - v_g) + p \end{bmatrix},$$

$$[\boldsymbol{e}_v, \boldsymbol{f}_v] = -\left(\frac{1}{\mathrm{Re}} + v_t\right) \begin{bmatrix} 0 & 0 \\ 2u_x & u_y + v_x \\ u_y + v_x & 2v_y \end{bmatrix}. \tag{17}$$

In equation (17), u, v and u_g, v_g are the Cartesian components of fluid and grid velocities, respectively. p is the pressure and β is a positive constant of artificial compressibility. All the variables are made dimensionless using the atmospheric air density ρ_a, the equilibrium

leakage velocity V_{A0}, and the bag length L_B. Re is the Reynolds number defined as $V_{A0}L_B/\nu$, where ν is the kinematic viscosity; ν_t is the nondimensional kinematic eddy viscosity determined from a turbulence model.

3.2. Spatial Discretization

A cell-centred finite-volume method is used for spatial discretization. The dependent variables $\boldsymbol{q}$ and the kinematic eddy viscosity ν_t are placed at the centre of each grid cell and the grid cell is treated as a control volume. The integration of flux is conducted using the Gauss integral theorem. Thus, the governing equations discretized in space are derived as follows:

$$\frac{\partial}{\partial t}(V\boldsymbol{q})_{i,j} + [\boldsymbol{E} + \boldsymbol{E}_v]_{i-1/2}^{i+1/2} + [\boldsymbol{F} + \boldsymbol{F}_v]_{j-1/2}^{j+1/2} = \boldsymbol{0}, \tag{18}$$

and

$$\begin{aligned} \boldsymbol{E} &= S_x^\xi \boldsymbol{e} + S_y^\xi \boldsymbol{f}, \qquad \boldsymbol{E}_v = S_x^\xi \boldsymbol{e}_v + S_y^\xi \boldsymbol{f}_v, \\ \boldsymbol{F} &= S_x^\eta \boldsymbol{e} + S_y^\eta \boldsymbol{f}, \qquad \boldsymbol{F}_v = S_x^\eta \boldsymbol{e}_v + S_y^\eta \boldsymbol{f}_v. \end{aligned} \tag{19}$$

In these equations, indices i and j are the cell numbering in curvilinear coordinates ξ and η, respectively, and $\pm\frac{1}{2}$ in the subscripts and overscripts correspond to the cell faces. V is a volume of the cell, and S_x, S_y are the area vector components of the cell boundaries.

The inviscid flux $\boldsymbol{E}$ is expressed as

$$\boldsymbol{E} = \begin{bmatrix} \beta U \\ u(U - U_g) + pS_x^\xi \\ v(U - U_g) + pS_y^\xi \end{bmatrix}, \tag{20}$$

where U and U_g are the fluid and grid contravariant velocity components in curvilinear coordinate direction ξ, respectively,

$$U = S_x^\xi u + S_y^\xi v, \qquad U_g = S_x^\xi u_g + S_y^\xi v_g. \tag{21}$$

The treatment of the grid velocity is described in Section 3.4.

The inviscid fluxes are discretized by the flux difference split scheme of Roe (1986). In the scheme, the numerical inviscid flux $\bar{\boldsymbol{E}}_{i+1/2}$ is given by

$$\bar{\boldsymbol{E}}_{i+1/2} = \tfrac{1}{2}[\boldsymbol{E}(\boldsymbol{q}^L) + \boldsymbol{E}(\boldsymbol{q}^R) - |\boldsymbol{A}|(\boldsymbol{q}^L - \boldsymbol{q}^R)]_{i+1/2}, \tag{22}$$

where $\boldsymbol{q}_{i+1/2}^L$ and $\boldsymbol{q}_{i+1/2}^R$ are the dependent variables extrapolated on the left and right sides of a cell face, respectively. $\boldsymbol{E}(\boldsymbol{q}^L)$ and $\boldsymbol{E}(\boldsymbol{q}^R)$ are evaluated from equation (20) with $\boldsymbol{q}^L$ or $\boldsymbol{q}^R$ and the area vectors. The Roe matrix $\boldsymbol{A}$ is the Jacobian of the inviscid flux $\boldsymbol{E}$ expressed as

$$\boldsymbol{A} = \frac{\partial \boldsymbol{E}}{\partial \boldsymbol{q}}. \tag{23}$$

In equation (23) the dependent variables at the cell face $\boldsymbol{q}_{i+1/2}$ are evaluated by Roe's averaging, namely the simple average of the right- and the left-side values. The eigenvalues

of the matrix $\boldsymbol{A}$ are U, $U + c_{ac}$, $U - c_{ac}$ where c_{ac} is the pseudo-speed of sound given by

$$c_{ac} = \sqrt{U^2 + \beta(S_x^2 + S_y^2)}. \tag{24}$$

With introduction of the right-eigenvector $\boldsymbol{R}$, the matrix $|\boldsymbol{A}|$ is expressed as

$$|\boldsymbol{A}| = \boldsymbol{R}|\boldsymbol{\Lambda}|\boldsymbol{R}^{-1}, \tag{25}$$

where $|\boldsymbol{\Lambda}|$ is

$$|\boldsymbol{\Lambda}| = \mathrm{diag}(|U|, |U + c_{ac}|, |U - c_{ac}|). \tag{26}$$

To attain third-order accuracy, the interface variables $\boldsymbol{q}^L$ and $\boldsymbol{q}^R$ are extrapolated by the MUSCL approach of Anderson *et al.* (1986) as

$$\begin{aligned} \boldsymbol{q}^L_{i+1/2} &= \boldsymbol{q}_i + \frac{\phi}{4}[(1-\psi)(\boldsymbol{q}_i - \boldsymbol{q}_{i-1}) + (1+\psi)(\boldsymbol{q}_{i+1} - \boldsymbol{q}_i)], \\ \boldsymbol{q}^R_{i+1/2} &= \boldsymbol{q}_{i+1} - \frac{\phi}{4}[(1-\psi)(\boldsymbol{q}_{i+2} - \boldsymbol{q}_{i+1}) + (1+\psi)(\boldsymbol{q}_{i+1} - \boldsymbol{q}_i)]. \end{aligned} \tag{27}$$

The above expression corresponds to the third-order accurate upwind-biased scheme with $\phi = 1$ and $\psi = \frac{1}{3}$. When $\phi = 0$ one obtains the first-order accurate upwind scheme. The numerical inviscid flux $\bar{\boldsymbol{F}}$ is evaluated in a similar manner.

Viscous fluxes are discretized by the second-order central differencing scheme based on the Gauss integral theorem.

3.3. Time Integration

The second-order accurate backward Euler formula is used for the time integration. To simplify the description of the process, consider the one-dimensional case of equation (18) which can be written as

$$\boldsymbol{N}(\boldsymbol{q}^{n+1}) \equiv \frac{3(V\boldsymbol{q})^{n+1} - 4(V\boldsymbol{q})^n + (V\boldsymbol{q})^{n-1}}{2\Delta t} + [\bar{\bar{\boldsymbol{E}}}^{n+1}]^{i+1/2}_{i-1/2} = \boldsymbol{0}, \tag{28}$$

where the numerical flux $\bar{\bar{\boldsymbol{E}}}$ is expressed as the sum of the numerical inviscid flux $\bar{\boldsymbol{E}}$ and the viscous flux $\boldsymbol{e}_v$. Equation (28) is solved by an approximate Newton relaxation method of Whitfield & Taylor (1991) as

$$\boldsymbol{N}'(\boldsymbol{q}^{n+1,m})\Delta\boldsymbol{q}^{n+1,m} = -\boldsymbol{N}(\boldsymbol{q}^{n+1,m}), \tag{29}$$

where

$$\Delta\boldsymbol{q}^{n+1,m} = \boldsymbol{q}^{n+1,m+1} - \boldsymbol{q}^{n+1,m}. \tag{30}$$

In these equations, m denotes the iteration index, and $\boldsymbol{N}'(\boldsymbol{q})$ is the Jacobian of the numerical flux vector with the first-order accurate upwind differencing. The resulting formulation of equation (29) is

$$\begin{aligned} &-\boldsymbol{\delta}_{i-1}\bar{\bar{\boldsymbol{E}}}_{i-1/2}\Delta\boldsymbol{q}^{n+1,m}_{i-1} + \boldsymbol{\delta}_{i+1}\bar{\bar{\boldsymbol{E}}}_{i+1/2}\Delta\boldsymbol{q}^{n+1,m}_{i+1} \\ &\quad + \left(\frac{3V_i^{n+1,m+1}}{2\Delta t}\boldsymbol{I} - \boldsymbol{\delta}_i\bar{\bar{\boldsymbol{E}}}_{i-1/2} + \boldsymbol{\delta}_i\bar{\bar{\boldsymbol{E}}}_{i+1/2}\right)\Delta\boldsymbol{q}^{n+1,m}_i \\ &\quad = -\left[\frac{3(V\boldsymbol{q})^{n+1,m}_i - 4(V\boldsymbol{q})^n_i + (V\boldsymbol{q})^{n-1}_i}{2\Delta t}\boldsymbol{I}_a + [\bar{\bar{\boldsymbol{E}}}^{n+1,m}]^{i+1/2}_{i-1/2}\right], \end{aligned} \tag{31}$$

where

$$\boldsymbol{\delta}_{i-1}\bar{\bar{\boldsymbol{E}}}_{i-1/2} = \frac{\partial \bar{\bar{\boldsymbol{E}}}^{n+1,m}_{i-1/2}}{\partial \boldsymbol{q}^{n+1,m}_{i-1}}. \tag{32}$$

In equation (31), $\boldsymbol{I}_a$ is the 3×3 identity matrix except the first diagonal element which is zero in order to satisfy the incompressible continuity equation. Equation (31) is solved with the initial value of $\boldsymbol{q}^{n+1,1} = \boldsymbol{q}^n$ at each time step, and the generated sequence $\boldsymbol{q}^{n+1,m+1}$ converges to $\boldsymbol{q}^{n+1}$, hence equation (28) is satisfied.

At each step of the Newton iteration, a large sparse linear system of equations has to be solved. In the present work, a symmetric Gauss–Seidel (sGS) relaxation approach is adopted.

3.4. Geometrical Conservation Law

For the resulting time integration to be conservative on a moving grid system, we must consider conservation of volume, which means that equation (18) should be satisfied on a moving grid in a uniform flow. When the grid moves and deforms in a uniform flow, the fluxes corresponding to a non-moving grid cancel out and then equation (18) becomes

$$\frac{3V^{n+1} - 4V^n + V^{n-1}}{2\Delta t} - [U_g^{n+1}]_{i-1/2}^{i+1/2} - [V_g^{n+1}]_{j-1/2}^{j+1/2} = 0, \tag{33}$$

where V_g is the grid velocity component in curvilinear coordinate direction η.

Next, the change of the volume is expressed as the sum of contributions from the movement of the each cell surfaces ΔV^{ξ}, ΔV^{η} as illustrated in Figure 3,

$$V^{n+1} = V^n + [\Delta V^{\xi^{n+1}}]_{i-1/2}^{i+1/2} + [\Delta V^{\eta^n}]_{j-1/2}^{j+1/2}. \tag{34}$$

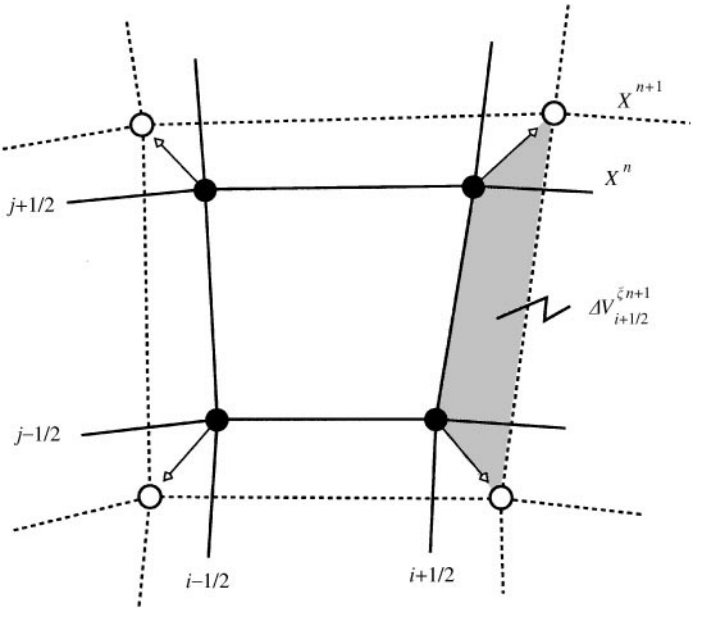

Figure 3. Geometrical conservation law (GCL).

Then, equation (33) can be written as

$$U^{n+1}_{g_{i+1/2}} = \frac{3\Delta V^{\xi^{n+1}}_{i+1/2} - \Delta V^{\xi^n}_{i+1/2}}{2\Delta t} \tag{35}$$

and

$$V^{n+1}_{g_{j+1/2}} = \frac{3\Delta V^{\eta^{n+1}}_{j+1/2} - \Delta V^{\eta^n}_{j+1/2}}{2\Delta t}. \tag{36}$$

The equations above are called the integral form of the "geometric conservation law" (GCL) by Thomas & Lombard (1978), since they deal with geometric properties and have the same general form as the integral statement of mass conservation. The grid velocities U_g and V_g in equation (20) are evaluated from equations (35) and (36).

3.5. Turbulence Model

The closure of the system of equations is achieved by introducing an algebraic two-layer turbulence model proposed by Baldwin & Lomax (1978). The kinematic eddy viscosity is given by

$$\nu_t = \begin{cases} (\nu_t)_{\text{inner}}, & y \le y_c, \\ (\nu_t)_{\text{outer}}, & y > y_c, \end{cases} \tag{37}$$

where y and y_c are the normal distance to the wall and the y coordinate where $(\nu_t)_{\text{inner}} = (\nu_t)_{\text{outer}}$, respectively.

In the inner region, $(\nu_t)_{\text{inner}}$ is given by the Prantl–Van Driest formulation as

$$(\nu_t)_{\text{inner}} = l^2|\omega|, \tag{38}$$

where $|\omega|$ is the vorticity magnitude and

$$l = \kappa y\left[1 - \exp\left(-\frac{y^+}{A^+}\right)\right]; \tag{39}$$

y^+ is the distance to the wall in wall units.

In the outer region, the following expression is used:

$$(\nu_t)_{\text{outer}} = KC_{cp}F_{\text{wake}}F_{\text{kleb}}, \tag{40}$$

where K and C_{cp} are constants. F_{wake} is defined as

$$F_{\text{wake}} = \min\left(y_{\max}F_{\max}, C_{wk}\frac{y_{\max}U^2_{\text{dif}}}{F_{\max}}\right). \tag{41}$$

$F_{\max}$ is the maximum value of the following function $F(y)$,

$$F(y) = y|\omega|\left[1 - \exp\left(-\frac{y^+}{A^+}\right)\right], \tag{42}$$

and $y_{\max}$ is the y coordinate where $F = F_{\max}$. U_{dif} is the difference of the maximum and the minimum velocity magnitudes in the profile. F_{kleb} is the Klebanoff intermittency factor given by

$$F_{\text{kleb}} = \left[1 + 5{\cdot}5\left(\frac{C_{\text{kleb}}y}{y_{\max}}\right)^6\right]^{-1}. \tag{43}$$

The model constants appearing in the foregoing relations are as follows:

$$A^+ = 26, \quad C_{cp} = 1{\cdot}6, \quad C_{\text{kleb}} = 0{\cdot}3, \quad C_{wk} = 1{\cdot}0,$$

$$\kappa = 0{\cdot}41, \quad K = 0{\cdot}0168.$$

The value of C_{wk} is modified from the original value (0·25) as suggested by Renze *et al.* (1992).

3.6. Boundary Conditions and Computational Grid

At the inflow boundary, the velocity is specified as

$$u_{\text{inflow}} = \frac{V_A H_L}{V_{A0} H_C}, \quad v_{\text{inflow}} = 0, \tag{44}$$

and the zero-extrapolation scheme is used for the pressure. At the outflow boundary, zero-extrapolation for the velocities and $p = 0$ are given. At the bottom boundary and on the wet-deck, the free slip condition with consideration of the movement of the free-surface due to the incident waves or the motion of the SES, is imposed. On the bag surface, a solid condition with grid velocities due to the SES motion is adopted. At the outer boundary, all dependent variables are extrapolated by the zero-extrapolation scheme.

Figures 4 and 5 illustrate the computational grid around a bag at a gap height of 30 mm. The air flows from the right side in these figures. The computational grid is body fitted to facilitate the implementation of boundary conditions. The mesh contains 89 planes

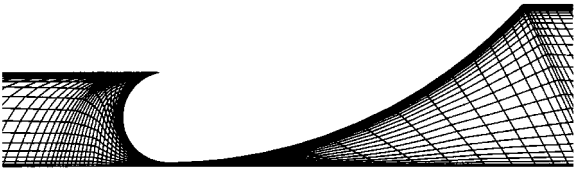

Figure 4. Initial computational grid at $H_L = 30$ mm.

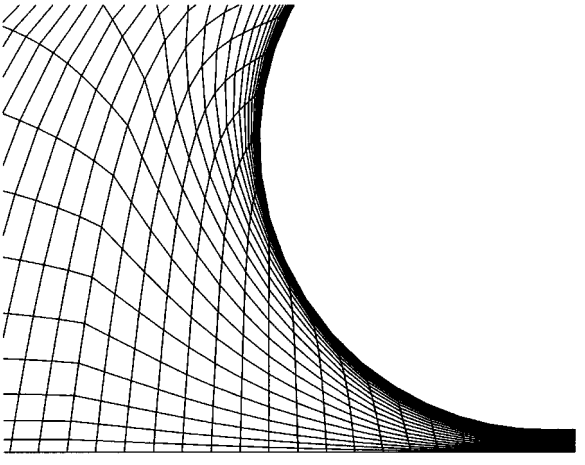

Figure 5. Enlarged view of initial computational grid.

streamwise and 49 vertically. The minimum spacings are 0·005 (17 mm) and $2{\cdot}1 \times 10^{-6}$ (0·007 mm) in the streamwise and the vertical directions. The grid points are clustered near the bag and the free-surface.

The solution domain extends two bag lengths upstream from the leading edge of the bag and an equal distance downstream from the trailing edge of the bag.

4. RESULTS AND DISCUSSION

4.1. Computational Conditions

Table 1 lists the principal particulars of a 30 m long class SES and data used in the present numerical simulation. Almost 80% of the weight is supported with the pressurized air-cushion and the leakage height at the stern, H_L, is only 30 mm.

The incident wave elevation is implied by equation (11). A head sea condition is considered and the peak period T_p is set to 1·8 s. Consequently, the peak encounter period T_e becomes 0·2 s, which corresponds to the first spatial resonance frequency of the cushion. The significant wave height is just 10 mm, since the present method does not allow the bag of the SES to touch the free-surface.

The equation system of SES motions and cushion pressure is solved with a coupling of the leakage flow solver for the four cases summarized in Table 2. In Case 1, leakage velocity

Table 1

Principal particulars of the SES

Weight (M)	140 000 kg
Moment of inertia (I_5)	6 860 000 kg m^2
Cushion length (L_C)	28 m
Cushion height (H_C)	1·368 m
Cushion beam (B_C)	8 m
Mean side-hull beam (b)	1·5 m
Mean side-hull sectional area coef.(s)	0·5
Mean cushion pressure (P_{C0})	5000 Pa
Mean fan flow rate (Q_{i0})	2·8 m^2/s
Cushion fan slope ($\partial Q/\partial P$)	$-$ 0·00104 m^{2}s/kg
X coordinate of fans (X_f)	12 m
Height of bag (H_B)	1·338 m
Length of bag (L_B)	3·489 m
Radius of curvature (R_1)	4.260 m
Radius of curvature (R_2)	0·387 m
Jet contraction at bow (k_{FE})	0·611
Jet contraction at stern (k_{AE})	0·963
Forward speed (U)	23·15 m/s

Table 2

Computed conditions

	Leakage velocity	Pressure on the bag
Case 1	$V_A = V_{A0}$	$P_B = P_C$
Case 2	Equation (14)	$P_B = P_C$
Case 3	Equation (14)	Equation (15)
Case 4	Equation (14)	N–S equations

and height are constant. Case 2 involves a variable leakage velocity and height effect, however the pressure distribution on the bag is not taken into account. Both Cases 3 and 4 consider the leakage effect and varying pressure distribution on the bag. The difference between them is whether viscous effects are involved or not. In the viscous numerical simulation (Case 4), the Reynolds number is set to $2{\cdot}2 \times 10^7$.

4.2. Equilibrium Flow Under a Bag

As described in Section 2, the equations of motion are calculated from the equilibrium condition. Hence, all cases require information on the equilibrium flow around the bag as an initial condition.

Figure 6 shows the computed velocity vectors for Case 4. The leakage flow comes from the right-hand side in the figure. At the lowest point of the bag, the velocity becomes

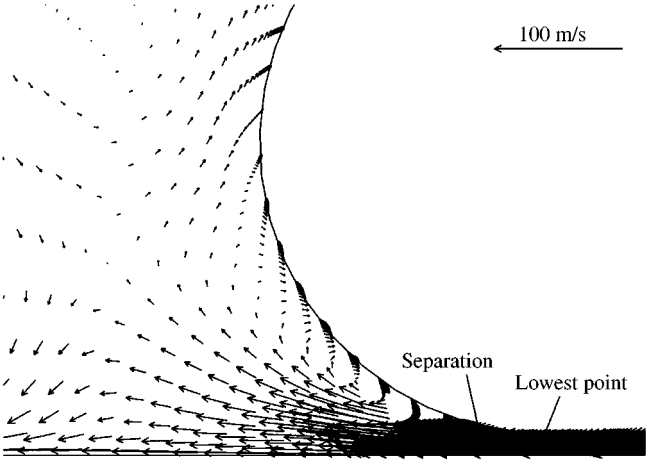

Figure 6. Initial velocity vector maps.

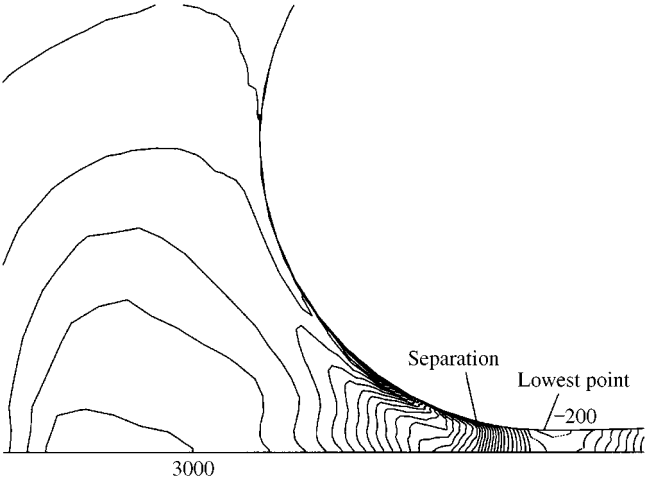

Figure 7. Contour maps of initial pressure distribution. Contour interval is 100 Pa. Dotted lines show negative values.

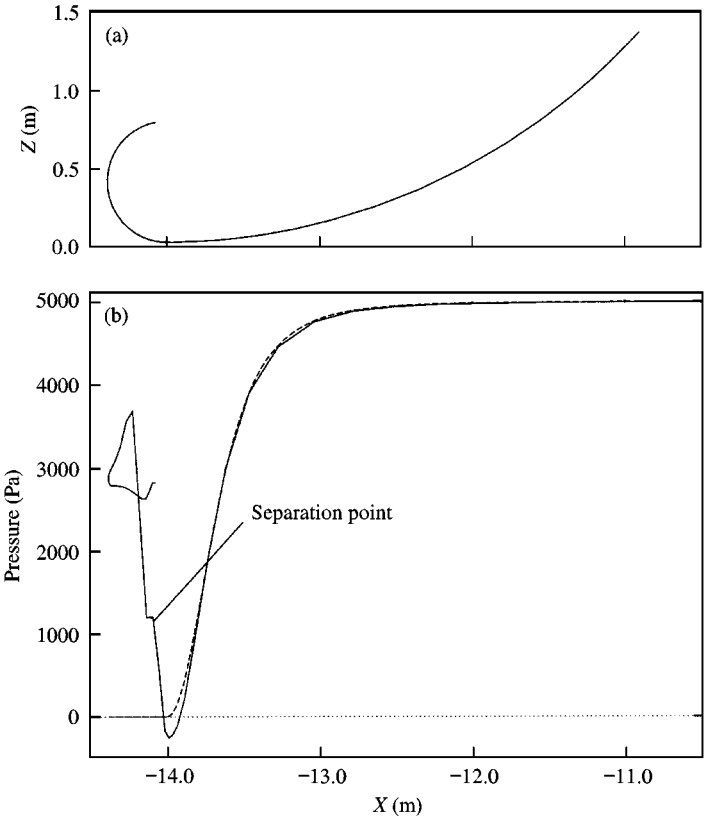

Figure 8. (a) Bag configuration (Z versus X) (b) Pressure distribution on a bag: ——, NS computation; ...., equation (15).

a maximum, approximately 93 m/s. After the air flows under the lowest point, the flow spreads, although a large separation occurs over the bag.

Figure 7 depicts the computed pressure distribution for Case 4. In order to set the computational pressure to the cushion pressure at the leading edge of the bag, a constant value is added to the computed one. In the region where the ground height is very small, the flow is almost a one-dimensional flow similar to the flow in the ground-effect mode. Behind the lowest point of the bag, the pressure recovers significantly.

Figure 8 shows the comparison of the viscous and inviscid pressure distributions on the bag. The lowest point of the bag is located at $X = -14$ m and the leading edge of the bag is at $X = -10{\cdot}83$ m. Around the lowest point, the present method provides a smaller pressure than that from the inviscid solution, because of the displacement effect due to the boundary layers developed over the bag. Behind the lowest point, the pressure from the inviscid solution is almost zero since the flow is assumed to shift to a jet at the lowest point. In contrast, the viscous flow solver simulates the pressure recovery due to the diffuser flow, approximately 1300 Pa, before the separation at $X = -14{\cdot}09$ m. Behind the separation, the flow is considered to change to jet flow, although the computed results cannot simulate the behaviour of the jet, owing to the lack of a turbulence model for the jet flow. The pressure recovery before the separation is expected to contribute to more realistic simulations of the bag deformation problem. However, detailed description of the flow requires a turbulence model tuned with use of measured data.

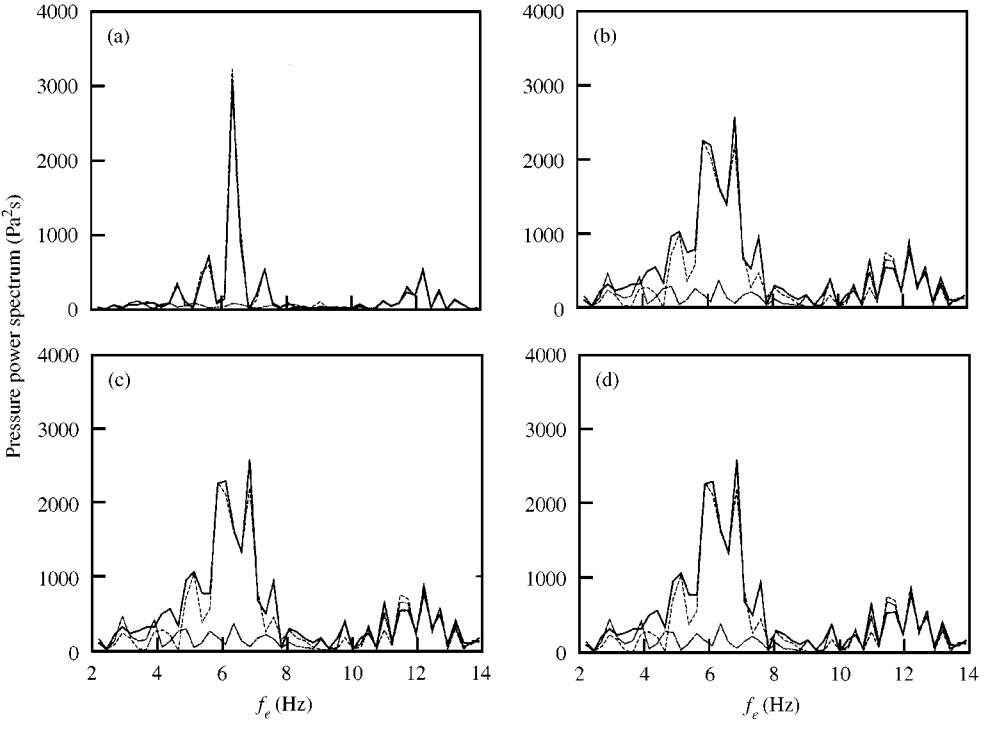

Figure 9. Spectra for cushion pressure: (a) Case 1; (b) Case 2; (c) Case 3; (d) Case 4. ——, at forward perpendicular (FP); ...., at centre of gravity (CG); - - -, at aft perpendicular (AP).

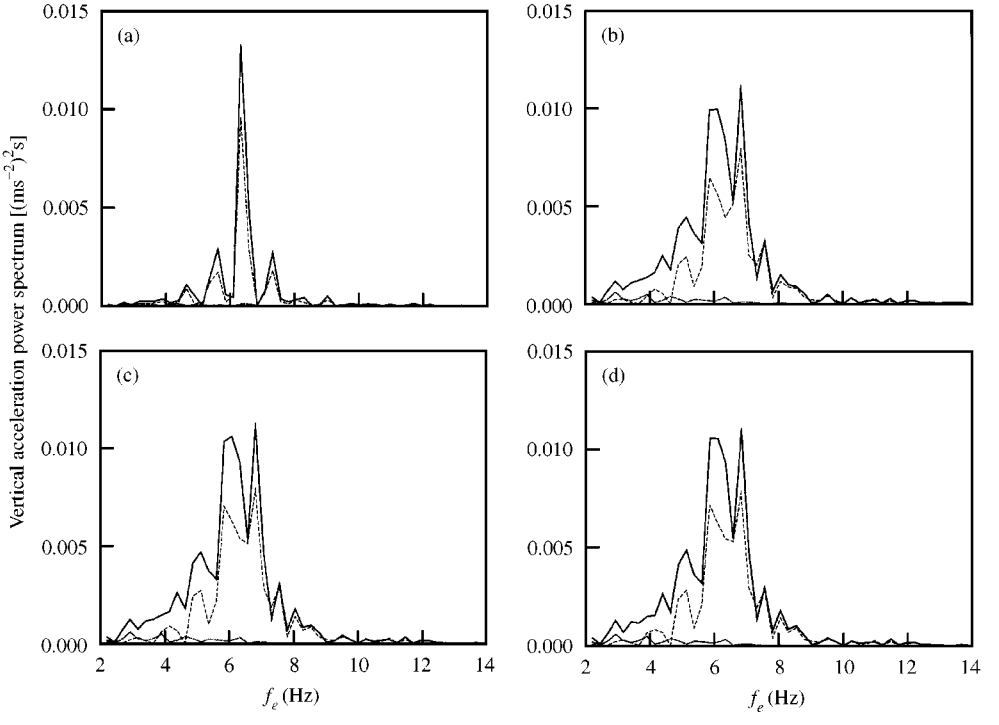

Figure 10. Spectra for vertical acceleration (a)–(d) as in Figure 9.

4.3. Effects on Cushion Pressure

Figures 9 and 10 show the unsteady cushion pressure and the vertical acceleration spectra at FP, CG and AP for all cases. In the pressure spectra for Case 1, two peaks can be observed around approximately 6 and 12 Hz which correspond to the first and second spatial resonances of a rectangular box with the cushion length of 28 m. The pressure at CG does not have the peak around 6 Hz because the frequency is a pitch motion mode. Spectra of the vertical acceleration have similar trends to that of the pressure.

First, we compare Cases 1 and 2. The cushion supported with the leakage effect leads to the large oscillations, relative to the cushion supported without this effect. This may be explained by the interaction between cushion pressure and varying pressure due to the leakage effect.

Next, three cases (Cases 2, 3 and 4) are compared. The difference between their conditions is the treatment of the bag forces. The bag forces do not affect the vertical motion itself directly, since the length of the bag is very small compared with that of the cushion.

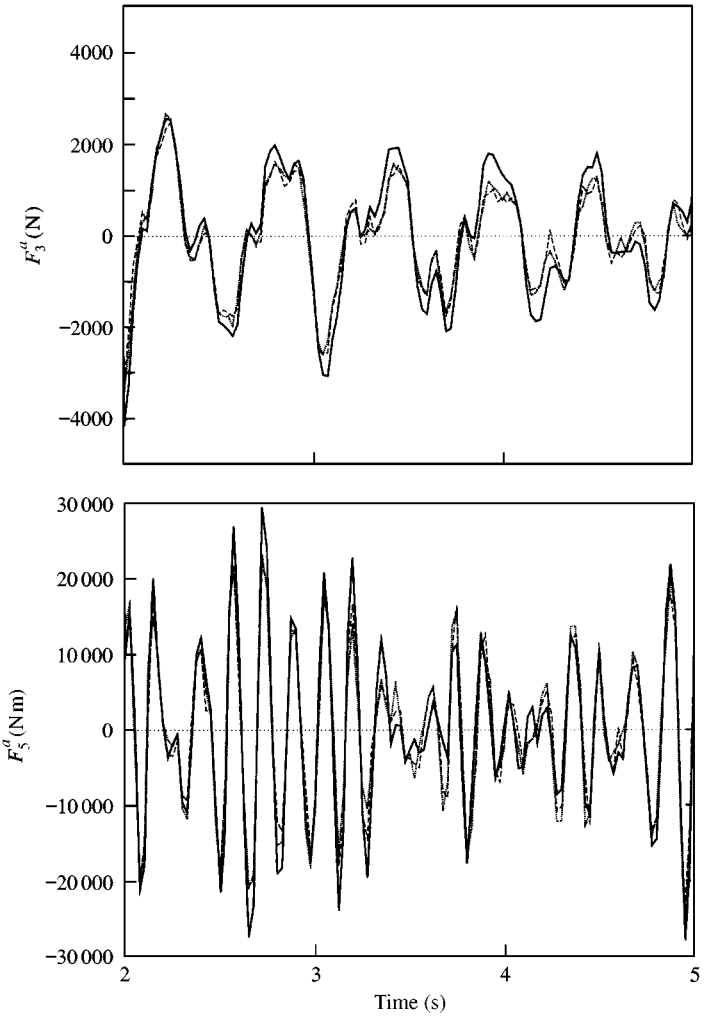

Figure 11. Time histories of (a) vertical force on the SES, F_3^a and (b) pitching moment on the SES, F_5^a :——, Case 2; . . . . , Case 3; - - - -, Case 4.

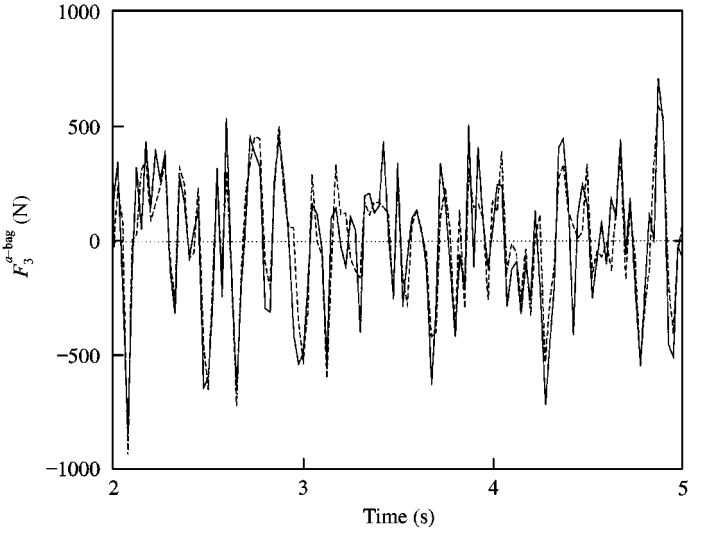

Figure 12. Time histories of vertical force on the bag, $F_3^{a-\text{bag}}$:——, Case 3; - - - -, Case 4.

Figure 11 depicts the comparison of the time histories of the aerodynamic forces acting on the SES. Although Case 2 differs slightly from the others, Cases 3 and 4 are almost the same in relation to the total aerodynamic forces.

Figure 12 shows the comparison of the time histories of the bag force. Some discrepancies can be seen between Case 3 and 4 due to the pressure recovery.

5. CONCLUSION

In order to obtain the pressure distribution on a stern seal bag of an SES with consideration of viscous effects, a two-dimensional time-dependent incompressible Navier–Stokes solver was developed using the finite-volume method on a moving grid system. The method was applied to the cobblestone effect problem for a 30 m long class SES with rigid stern seal bag. Results were compared with the data using the inviscid method by Ulstein, and the pressure recovery from the lowest point of the bag to the separation point could be seen in the viscous flow investigation. For the cushion supported with a rigid stern seal, the viscous effect was not so significant. However, for the cushion supported with a flexible stern seal, the recovery due to the viscous effect is expected to contribute to more realistic estimation of both the bag deformation and the global motion.

Future plans include the introduction of jet phenomena and consideration of the flexible bag motion.

References

Anderson, W. K., Thomas, J. L. & Van Leer, B. 1986 Comparison of finite volume flux vector splitting for the euler equations. AIAA Journal **24,** 1453–1460.

Baldwin, B. S. & Lomax, H. 1978 Thin-layer approximation and algebraic model for separated turbulent flows. AIAA paper **78-257**.

Renze, K. J., Buning, P.G. & Rajagopalan, R. G. 1992 A comparative study of turbulence models for overset grids. AIAA paper **92-0437**.

Roe, P. L. 1986 Characteristic-based schemes for the euler equations. *Annual Review of Fluid Mechanics* **18,** 337–365.

Thomas, P. D. & Lombard, C. K. 1978 Geometric conservation law and its application to flow computations on moving grids. *AIAA Journal* **17,** 1030–1037.

Ulstein, T. 1995, Nonlinear effects of a flexible stern seal bag on cobblestone oscillations of an SES. Dr.ing thesis, Norwegian Institute of Technology.

Whitfield, D. L. & Taylor, L. K. 1991 Discretized Newton-relaxation solution of high resolution flux-difference split schemes. AIAA paper **91-1539CP**, pp. 134–145.